Enhanced efficiency of inverted polymer solar cells using two-step sputtered ZnO as cathode interfacial layer

2014 Mater. Res. Express 1 025020

(http://iopscience.iop.org/2053-1591/1/2/025020)

Materials Research
Express

Enhanced efficiency of inverted polymer solar cells using two-step sputtered ZnO as cathode interfacial layer

Feng Zhu[1], Xiaohong Chen[1], Jianping Zhou[2], Zhe Lu[1], Yiwei Chen[1], Sumei Huang[1] and Zhuo Sun[1]

[1] Engineering Research Center for Nanophotonics and Advanced Instrument, Ministry of Education, and Department of Physics, East China Normal University, Shanghai 200062, People's Republic of China
[2] School of Power and Automation Engineering, Shanghai University of Electric Power, Shanghai 200090, People's Republic of China
E-mail: xhchen@phy.ecnu.edu.cn

Received 19 March 2014, revised 8 April 2014
Accepted for publication 10 April 2014
Published 7 May 2014

Materials Research Express **1** (2014) 025020
doi:10.1088/2053-1591/1/2/025020

Abstract

Efficient inverted polymer solar cells (PSCs) with two-step deposited zinc oxide (ZnO) cathode interfacial layer are developed by magnetron sputtering method. The first-step ZnO layer sputtered with Ar gas has lower bulk resistance due to increasing oxygen vacancy. The second-step ZnO layer sputtered with O_2/Ar ratio (1:7) gas can obtain lower contact barrier and superior interface properties at ZnO/photoactive layer interface. The power conversion efficiencies of inverted poly(3-hexylthiophene) and phenyl-C61-butyric acid methylester (P3HT:PCBM) based PSCs with 11 nm/4 nm and 50 nm/10 nm ZnO layers are, respectively, 4.08% and 3.13%, which are obviously higher than that of corresponding PSCs with O_2/Ar gas sputtered 15 nm and 60 nm ZnO layers. The conduction band level of ZnO film with O_2/Ar sputtering gas is higher, 0.14 eV, than that of ZnO film with only Ar layer derived from ultraviolet photoelectron spectroscopy and optical band gap of ZnO films. The capacitive behavior of PSCs with 30 nm and 60 nm layers indicates that two-step sputtered ZnO layer can efficiently enhance electron transport ability of bulk ZnO layer and attenuate electron accumulation at ZnO/P3HT:PCBM interface. Lower reverse saturation current and higher shunt resistant of PSCs with two-step sputtered ZnO layer demonstrated that the defects penetrating into the whole ZnO layer can be inhibited.

Keywords: polymer solar cells, magnetron sputtering deposition, zinc oxide, capacitance

1. Introduction

Polymer solar cells (PSCs) need to develop high power conversion efficiency (PCE), long lifetime, light weight, low price and flexibility to meet market applications [1]. Low band-gap polymers, good bulk heterojunction structure and superior interface contact are all effective methods to improve performance of PSCs [2–5]. The PCEs of PSCs have been quickly increased in the past few years, reaching 8–10% for both conventional and inverted PSC structures [6–9]. In conventional PSCs, the acidic poly(3,4-ethylenedioxythiophene)/poly(styrenesulfonate) (PEDOT:PSS) and low work function metals such as Al and Ca/Ag usually act as an anode interfacial layer and cathode, respectively. The acidic PEDOT:PSS layer is detrimental to ITO anode and low work function metal cathodes are easily oxidized, leading to reducing device lifetime [10]. The inverted PSCs have more advantages over conventional PSCs to inhibit electrode oxidation and degradation [11]. The PCEs of inverted PSCs comparable to conventional PSCs are primarily attributed to the selection and optimization of n-type and p-type selective layers.

To gain efficient inverted PSCs, inorganic metal oxides such as TiO_2 and ZnO, and organic materials such as poly [(9,9-bis (3′-(N,N-dimethylamino) propyl) -2,7-fluorene) -alt-2,7- (9,9– dioctyl -fluorene)] and ionic liquid-functionalized carbon nanoparticles as a cathode interfacial layer have extensively been studied [7, 11–13]. Among these materials, ZnO is well-known as a good cathode interfacial material due to high transparency in the visible and near infrared wavelength range. Compared to frequently used TiO_2 material, ZnO has higher electron mobility, which results in lower series resistance and flexibly designed thickness of ZnO layer in PSCs [14]. However, PCEs of PSCs are closely related to synthetic ZnO methods and fabrication process of PSCs. For a sol–gel derived ZnO layer, high-temperature annealing is required to thermally decompose zinc acetate precursor, which hinders the use of flexible substrates and low-cost roll-to-roll processes [11]. Therefore, developing a high quality ZnO layer at low temperature is significant for PSC industrial applications. The solution-processed ZnO nanoparticles have demonstrated good electron mobility without additional thermal annealing [15]. Nevertheless, this progress in wet process cannot exclude the development of dry deposition technologies used in production to grow interfacial layers for PSCs. ZnO cathode interfacial layer in PSCs has been reported by plasma enhanced chemical vapor deposition [16], atomic layer deposition [17] and magnetron sputtering deposition [18–20]. Magnetron sputtering technique can precisely control film composition and thickness, and is easily compatible with roll-to-roll coating processes and tin-doped indium oxide (ITO) and aluminum-doped zinc oxide (AZO) fabrication procedures. Moreover, directional deposition film can avoid the pollution of the substrate back during roll-to-roll coating processes [21]. Considering present commercial ITO and AZO transparent conducting films and universal emerging metal-oxide/metal/metal-oxide films [22, 23], fabricated with magnetron sputtering technology, developing a sputtered ZnO layer in PSCs is helpful to be compatible with the procedure of transparent conducting film and to control cost of PSCs.

Sputtered ZnO film as cathode interfacial layer has been applied to conventional and inverted PSCs [18, 24]. In conventional PSCs, the photoactive layer/ZnO layer interface morphology can be changed during sputtering process, which results in high interface contact barrier and low PCE of PSCs. The performance of PSCs is improved to some extent by strictly controlling ZnO sputtering condition and annealing condition of PSCs [24]. Similarly, the surface morphology and crystalline quality of ZnO layer can significantly influence performance of inverted PSCs [18, 20]. Sputtering condition (such as RF power, O_2/Ar ratio, work pressure and substrate temperature), thickness of film and thermal annealing condition can usually adjust the crystalline quality and stoichiometry of ZnO films, which change the optical and electrical properties of ZnO film [25]. The high substrate temperature and post annealing temperature are not recommended for sputtered ZnO film on flexible substrates. Without substrate temperature, Jouane *et al* reported inverted PSCs using sputtered ZnO as cathode interfacial layer deposited on glass and poly(ethylene glycol)2,6-naphthalate substrates, respectively [18]. However, PSCs showed low PCE and moderate annealing temperature (160 ~ 180 °C) was further used to improve ZnO structural properties and the performance of PSCs. In this paper, two-step sputtered ZnO layer as cathode interfacial layer was deposited on ITO/glass substrate without substrate temperature by magnetron sputtering method. The first-step sputtered ZnO layer was deposited with only Ar sputtering gas to decrease ZnO bulk resistance due to increasing oxygen vacancies. The second-step ZnO layer with O_2/Ar mixture sputtering gas was deposited on top of the first-step sputtered ZnO layer to adjust interface properties between photoactive layer and ZnO layer. The PCE of PSCs is significantly improved after depositing a second-step ZnO layer compared to PSCs with single-step sputtered ZnO layer.

2. Experimental details

Regioregular poly(3-hexylthiophene) (P3HT) and [6,6]-phenl-C_{61}-butyric acid methyl ester (PCBM) were purchased and received without further purification. The PSCs were fabricated with a structure of ITO/ZnO/P3HT:PCBM/MoO_3/Al. The patterned ITO substrates were cleaned by ultrasonic bath treatment followed by detergent, de-ionized water, acetone, and isopropanol for 10 min, respectively. After being dried in air, ITO glass underwent ultraviolet-ozone treatment for 15 min before being transferred into the magnetron sputtering chamber. The ZnO layer was deposited with RF 50 W and working pressure 0.3 Pa under a base pressure of 1.1×10^{-5} Torr, using a commercial ZnO target of 99.99% purity. A total mixed gas flow of 20 sccm with different O_2/Ar ratio gas was kept in all sputtered samples. The sputtering rate of ZnO was fixed at 0.8 Å s^{-1}. The mixture solution of P3HT:PCBM (1:0.8) in dichlorobenzene was spin-coated on top of the ZnO surface at 800 rpm for 60 s, and then kept in a petri dish for slow growth. After placement in air for at least 5 h, P3HT:PCBM films were annealed at 120 °C in an oven for 10 min to remove the residual solvent. Finally, a 15 nm thick MoO_3 anode interfacial layer and 150 nm Al electrode were deposited on the P3HT:PCBM photoactive layer under a background pressure of 2.5×10^{-6} Torr. The thickness of P3HT:PC_{61}BM blended layer was about 180 nm, and the active area of the device was 0.10 cm^2. Current–voltage characteristics were measured under AM1.5G illumination intensity of 100 mW cm^{-2} using a Newport solar simulator system. All samples were measured in air without encapsulation. The surface morphologies of ZnO films were measured using atomic force microscopy (AFM, NanoWizard II). The work function of ZnO/ITO films was examined using ultraviolet photoelectron spectroscopy (UPS) with Helium line (21.2 eV).

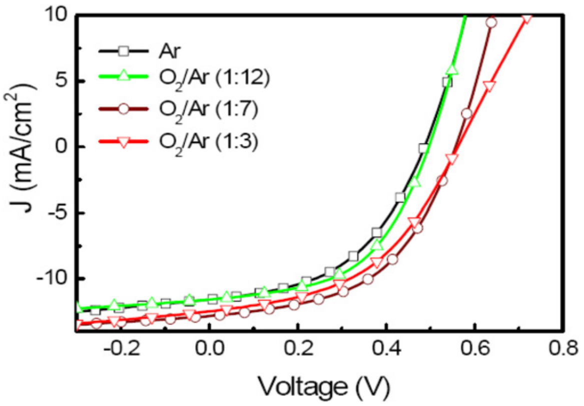

Figure 1. *J–V* curves of representative inverted PSCs with 15 nm ZnO layer sputtered with different O_2/Ar ratio gas.

Table 1. Parameters and scatter PCEs of inverted PSCs with 15 nm ZnO layer sputtered with different O_2/Ar ratio gas.

O_2/Ar ratio	V_{OC} (V)	J_{SC} (mA cm^{-2})	*FF*	*PCE* (%)	R_S ($\Omega\,cm^{-2}$)	R_{sh} ($\Omega\,cm^{-2}$)
Ar	0.49	11.5	0.48	2.74 (± 0.2)	10.8	238
1:12	0.49	11.5	0.52	2.98 (± 0.1)	10.6	309
1:7	0.56	12.4	0.51	3.63 (± 0.2)	10.6	279
1:3	0.56	12.4	0.47	3.31 (± 0.1)	15.5	309

3. Results and discussion

Figure 1 shows current density–voltage (*J–V*) curves of representative PSCs with 15 nm ZnO layer sputtered with different O_2/Ar ratio gas. The V_{oc}, J_{sc}, FF, PCE and serial resistance (R_s) and shunt resistance (R_{sh}) deduced from *J–V* curves are summarized in table 1. R_s and R_{sh} are derived from *J–V* curves at V_{oc} and 0 V, respectively. The V_{oc}, FF and PCE of PSCs with O_2/Ar ratio (1:7) sputtering gas are, respectively, 0.56 V, 0.51 and 3.63%, which are obviously higher than 0.49 V, 0.48 and 2.74% of PSCs with only Ar sputtering gas. The R_s of PSCs with O_2/Ar ratio (1:7) gas is 10.6 $\Omega\,cm^{-2}$, which is close to R_s (10.8 $\Omega\,cm^{-2}$) of PSCs with only Ar gas. However, the R_s of PSCs is quickly increased with O_2/Ar ratio increasing to 1:3 from 1:7. The R_s of PSCs with O_2/Ar ratio (1:3) gas is increased to 15.5 $\Omega\,cm^{-2}$. Accordingly, the PCE of PSCs is decreased to 3.31% from 3.63%. PSCs with O_2/Ar (1:7) sputtering gas showing better performance possibly have both low serial resistance and superior interface properties.

The serial resistance of PSCs is primarily from bulk resistance of P3HT:PCBM, ZnO and MoO_3 layers, electrodes and contact resistance between different layers. For a PSC with ZnO cathode interfacial layer system, the bulk resistance of ZnO layer would be decreased with reducing O_2/Ar ratio gas due to increasing oxygen vacancies [25]. However, the interface contact properties between ZnO and P3HT:PCBM layer are inferior, based on poor performance of PSCs with only Ar gas in figure 1 and table 1. To reduce bulk resistance of ZnO layer and obtain superior interface contact at ZnO/P3HT:PCBM interface, two-step

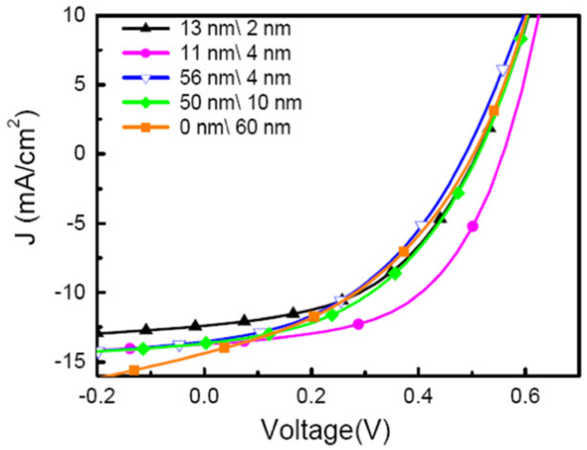

Figure 2. *J–V* curves of representative PSCs with two-step sputtered X (nm)\Y (nm) ZnO layer. X stands for first-step thickness of ZnO layer deposited with only Ar gas, and Y stands for second-step thickness of ZnO layer deposited with O_2/Ar (1:7) gas in all figures and tables.

Table 2. Parameters and scatter PCEs of inverted PSCs with two-step sputtered X (nm) \Y (nm) ZnO layer.

X(nm) \Y(nm)	V_{OC} (V)	J_{SC} (mA cm^{-2})	*FF*	*PCE* (%)	R_s (Ω cm^{-2})	R_{sh} (Ω cm^{-2})
13\2	0.51	12.3	0.47	3.00 (± 0.2)	12.0	235
11\4	0.56	13.7	0.53	4.08 (± 0.12)	8.4	343
56\4	0.47	13.4	0.43	2.73 (± 0.1)	12.8	198
50\10	0.51	13.6	0.45	3.13 (± 0.1)	12.5	225
0\60	0.50	14.3	0.40	2.65 (± 0.2)	13.2	103

sputtered ZnO layer is developed. Figure 2 shows *J–V* curves of representative PSCs with two-step sputtered ZnO layer. The first-step ZnO layer was deposited with Ar sputtering gas to increase oxygen vacancies [25]. The second-step ZnO layer was deposited with O_2/Ar ratio (1:7) gas to improve interface properties of ZnO layer. The corresponding parameters of representative PSCs deduced from *J–V* curves are summarized in table 2. The PCE (4.08%) of PSCs with two-step sputtered ZnO layer (11 nm/4 nm) is significantly higher than that of PSCs based on single-step sputtered 15 nm ZnO layer with O_2/Ar ratio (1:7) gas. Accordingly, the R_s of PSCs with 11 nm/4 nm ZnO layer is decreased to 8.4 Ω cm^{-2} from 10.6 Ω cm^{-2} of PSC with O_2/Ar single-step sputtered 15 nm ZnO layer. However, the V_{oc} (0.51 V) of PSCs with 13 nm/ 2 nm ZnO layer is obviously lower than that of PSCs with 11 nm/4 nm ZnO layer and O_2/Ar sputtered 15 nm ZnO layer. As for the thicker 60 nm ZnO layer, PSCs with 50 nm/10 nm ZnO layer have higher PCE (3.13%) and V_{oc} (0.51 V) and lower R_s (12.5 Ω cm^{-2}) compared to PSCs with 56 nm/4 nm and single-step sputtered 60 nm ZnO layers. This means that a 4 nm thick second-step ZnO layer better for totally thick 15 nm ZnO layer is too thin for totally thick 60 nm ZnO layer. The right thickness of the second-step ZnO layer is closely related to the first-step layer thickness to attain superior interface contact at ZnO/P3HT:PCBM interface.

The difference of interface contact at ZnO/photoactive layer usually affects carrier accumulation and transport in PSCs, which would be observed by impedance spectroscopy

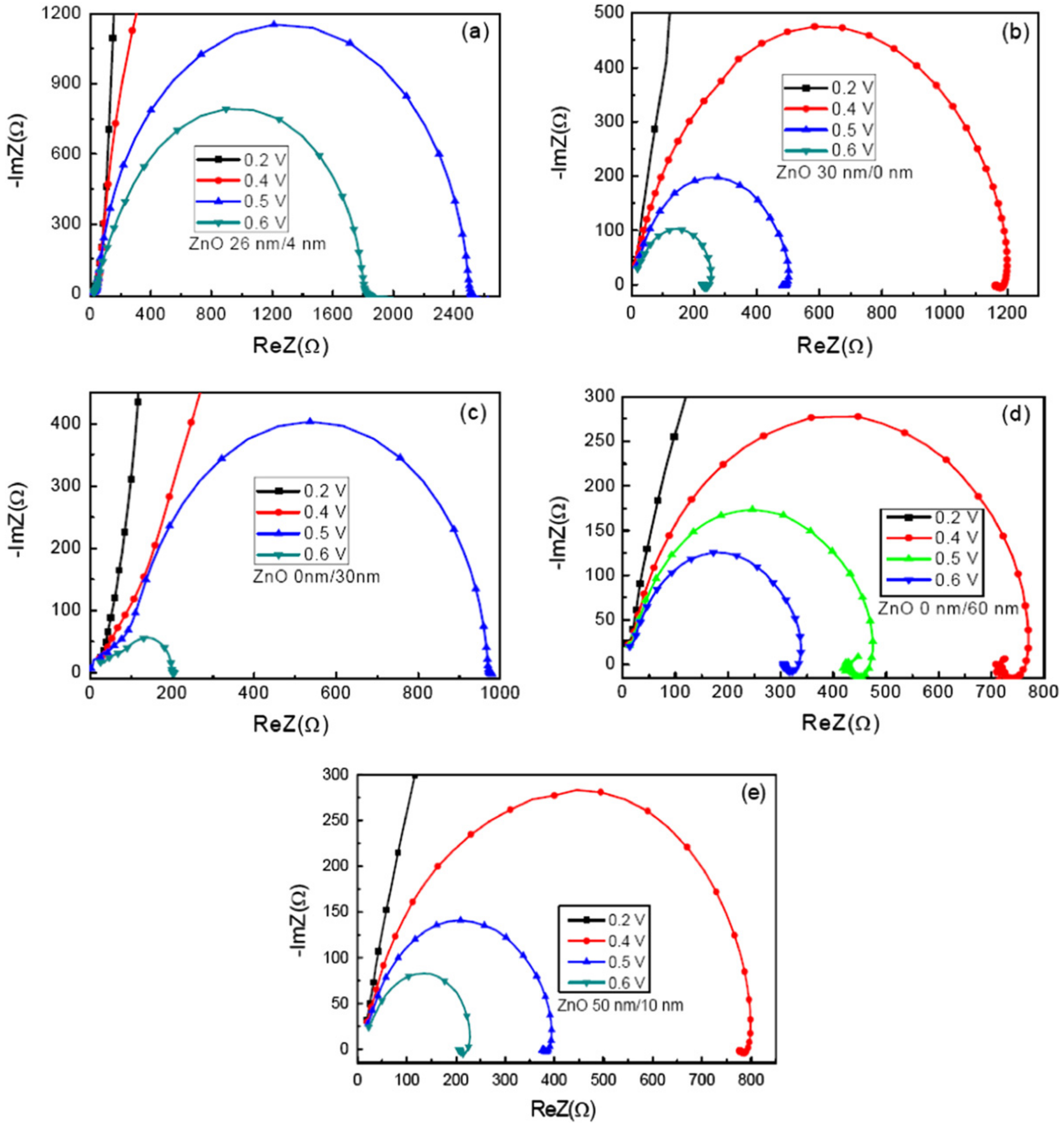

Figure 3. Bias dependence of Cole–Cole plots of inverted PSCs with two-step sputtered X (nm)\Y (nm) ZnO layer in the dark. Measured bias voltages are 0.2, 0.4, 0.5 and 0.6 V, respectively.

[26, 27]. Figure 3 shows impedance spectra of PSCs with ZnO layer in the dark. The –Im(Z) values excluding PSCs with Ar gas sputtered 30 nm ZnO layer are always positive for PSCs with 26 nm/4 nm ZnO layer and single-step sputtered 30 nm ZnO layer with O_2/Ar gas, as shown in figures 3(a)–(c). The slight negative capacitive behavior of PSCs with Ar gas sputtered 30 nm ZnO layer indicates that electrons are slightly accumulated at the ZnO/P3HT: PCBM interface due to high interface barrier [26]. That is to say, the two-step sputtered 26 nm/ 4 nm and O_2/Ar single-step sputtered 30 nm ZnO layers can result in lower interface barrier and

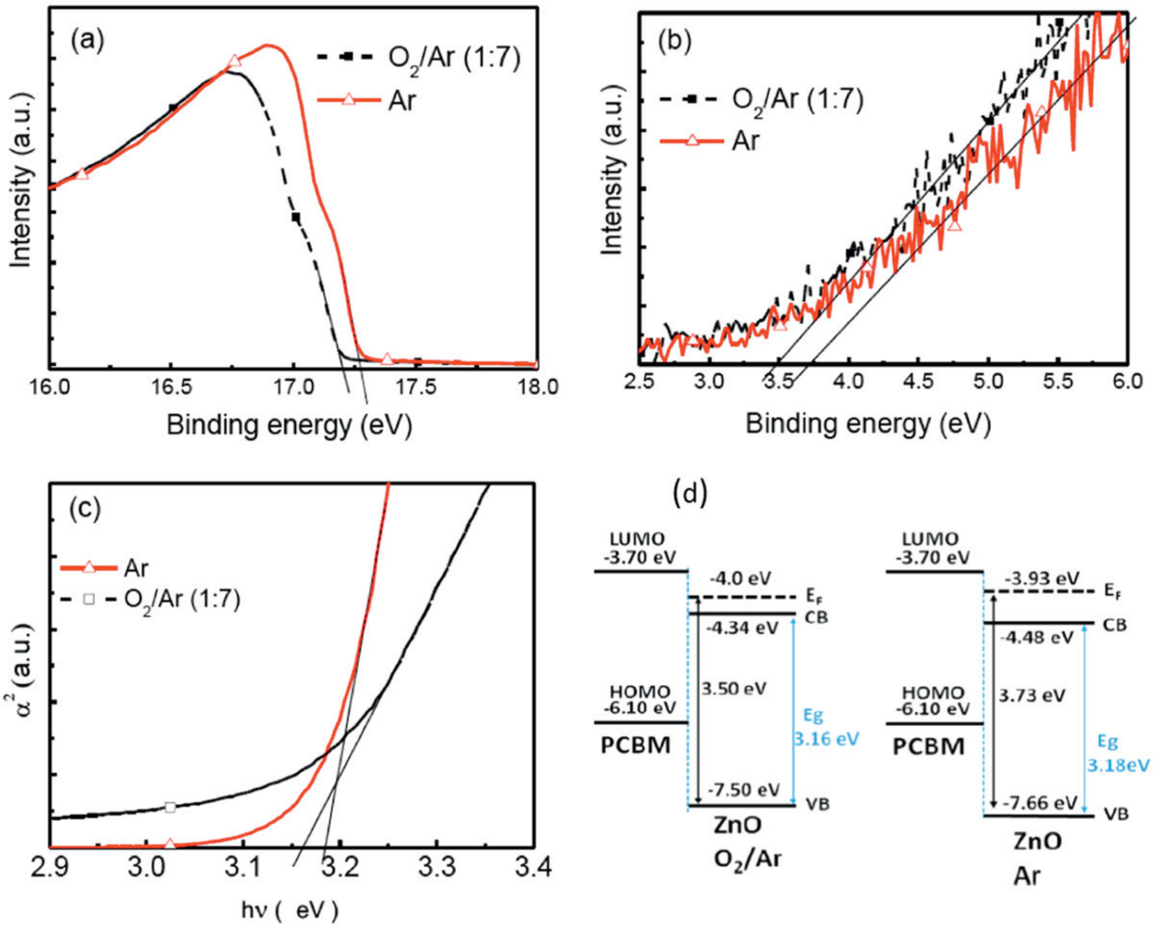

Figure 4. (a) UPS secondary electron emission cutoff measured for ZnO films with Ar and O_2/Ar gas. (b) UPS spectra of ZnO films, revealing the respective positions of ZnO valence band edge. (c) Optical band gap of ZnO films sputtered with Ar and O_2/Ar gas. (d) Energy level diagrams between PCBM and ZnO films derived from UPS spectra and optical band gap of ZnO films.

avoid obvious electron accumulation at the ZnO/P3HT:PCBM interface. The negative -Im(Z) values can still be observed for PSCs with 50 nm/10 nm and single-step O_2/Ar gas sputtered 60 nm ZnO layers, as illustrated in figures 3(d)–(e). However, the negative capacitance effect of PSCs with 50 nm/10 nm ZnO layer becomes much weaker compared to PSCs with single-step sputtered 60 nm ZnO layer. The slight negative capacitance effect suggests that two-step sputtered 50 nm/10 nm ZnO layer is more helpful to inject and transport electrons than single-step O_2/Ar sputtered 60 nm ZnO layer.

To understand the mechanism of two-step sputtered ZnO interfacial layer, UPS measurements were performed to determine the electronic structures on ZnO layer. Figure 4(a) shows the secondary electron emission cutoff in UPS spectra measured for ZnO films with Ar and O_2/Ar (1:7) sputtering gas. The 7 nm instead of 15 nm thick ZnO film was deposited onto ITO coated glass to favorably transfer electrons from ZnO surface to ITO and avoid electron accumulation in ZnO surface during UPS measurements. The 4.0 eV work function of ZnO surface with O_2/Ar (1:7) sputtering gas was increased 0.07 eV compared to

3.93 eV of ZnO with only Ar gas. The valence band (VB) edge was determined to be 3.73 eV below the Fermi level (E_F) of ZnO with Ar gas and 3.50 eV for ZnO with O_2/Ar gas, as shown in figure 4(b). Figure 4(c) shows the photon energy dependence of square absorption coefficient (α^2) for 120 nm thick ZnO films. The energy band gap (E_g) values extrapolated from the straight regions of the plots to $\alpha = 0$ were 3.16 eV and 3.18 eV for ZnO films with O_2/Ar and Ar sputtering gas. The estimated conduction band CB levels were −4.34 eV and −4.48 eV for ZnO with O_2/Ar and Ar gas based on these VB energies and optical band gaps [28]. The measured Fermi energy of ZnO located with the CB has been demonstrated by experiments and band-structure calculation [28–30]. The band alignment diagrams between PCBM and ZnO films are summarized in figure 4(d). The decreasing energy difference (0.14 eV) between LUMO of PCBM and CB of ZnO with O_2/Ar gas compared to ZnO with Ar sputtering gas indicated a lower contact barrier of the ZnO/P3HT:PCBM layer, which is consistent with increasing V_{oc} of PSCs with O_2/Ar gas sputtered ZnO layer. Although the CB energy level of 15 nm ZnO layer compared to a 7 nm ZnO film would be slightly different, a little difference (0.14 eV) of CB between ZnO layers sputtered with Ar and O_2/Ar gas cannot completely explain significantly enhancing PCE and V_{oc} of PSCs with 11 nm/4 nm ZnO layer compared to PSCs with Ar gas 15 nm ZnO layer, which means that other possible factors such as surface morphology and serial resistance may affect interface contact at the ZnO/P3HT:PCBM interface [31, 32].

Figure 5 shows AFM surface morphologies of ZnO films. The root-mean-square (RMS) roughness of 15 nm and 60 nm ZnO films with Ar sputtering gas are 2.12 nm and 4.45 nm, respectively. RMS roughness of 15 nm and 60 nm ZnO films with O_2/Ar (1:7) sputtering gas are 1.94 nm and 3.12 nm, respectively. Surface roughness of ZnO film is gradually increased with increasing ZnO film thickness. The rougher surface of the first-step ZnO layer usually needs the thicker second-step ZnO layer to avoid directly contact between P3HT:PCBM film and first-step ZnO layer. This can roughly explain why a 4 nm second-step ZnO layer better for totally thick 15 nm ZnO layer is too thin for totally thick 60 nm ZnO layer. In addition, surface morphology of ZnO films with O_2/Ar gas becomes smoother compared to correspondingly thick ZnO films with only Ar gas. Therefore, we can qualitatively speculate that the two-step sputtered ZnO layers compared to correspondingly thick ZnO layers with Ar sputtering gas have slightly smoother surface due to oxygen gas participation.

The seriously rough surface may result in deteriorated films and forms pinholes in the photoactive layer [19, 31, 32]. The reverse saturation current of PSCs compared to PSCs with Ar gas sputtered ZnO layer is obviously inhibited after the two-step sputtered ZnO layer, as shown in figure 6. PSCs with 60 nm ZnO layer sputtered with Ar or O_2/Ar gas shows higher reverse saturation current than that of PSCs with 50 nm/10 nm and 56 nm/4 nm ZnO layers. The obviously high reverse saturation and low shunt resistance, shown in table 2, of PSCs with 60 nm single-step sputtered ZnO layer are possibly attributed to serious roughness of ZnO layer, which easily results in defects of photoactive layer [32]. However, the reverse saturation current of PSCs with 11 nm/4 nm is lower than that of PSCs with single-step O_2/Ar sputtered 15 nm ZnO layer. In the meantime, the reverse saturation current of PSCs with 50 nm/10 nm ZnO layers is slightly lower than that of PSCs with 13 nm/2 nm and Ar sputtered 15 nm ZnO layers. The relatively lower reverse saturation current of PSCs with X (nm)/Y (nm) ZnO layer compared to PSCs with Ar sputtered 15 nm and 60 nm ZnO layers cannot be completely explained from the various roughness of ZnO layer. In fact, perfect ZnO layer can also inhibit reverse current and improve shunt resistance of PSCs. The surface morphologies of the same thick ZnO films sputtered with O_2/Ar and Ar gas are obviously different from AFM images.

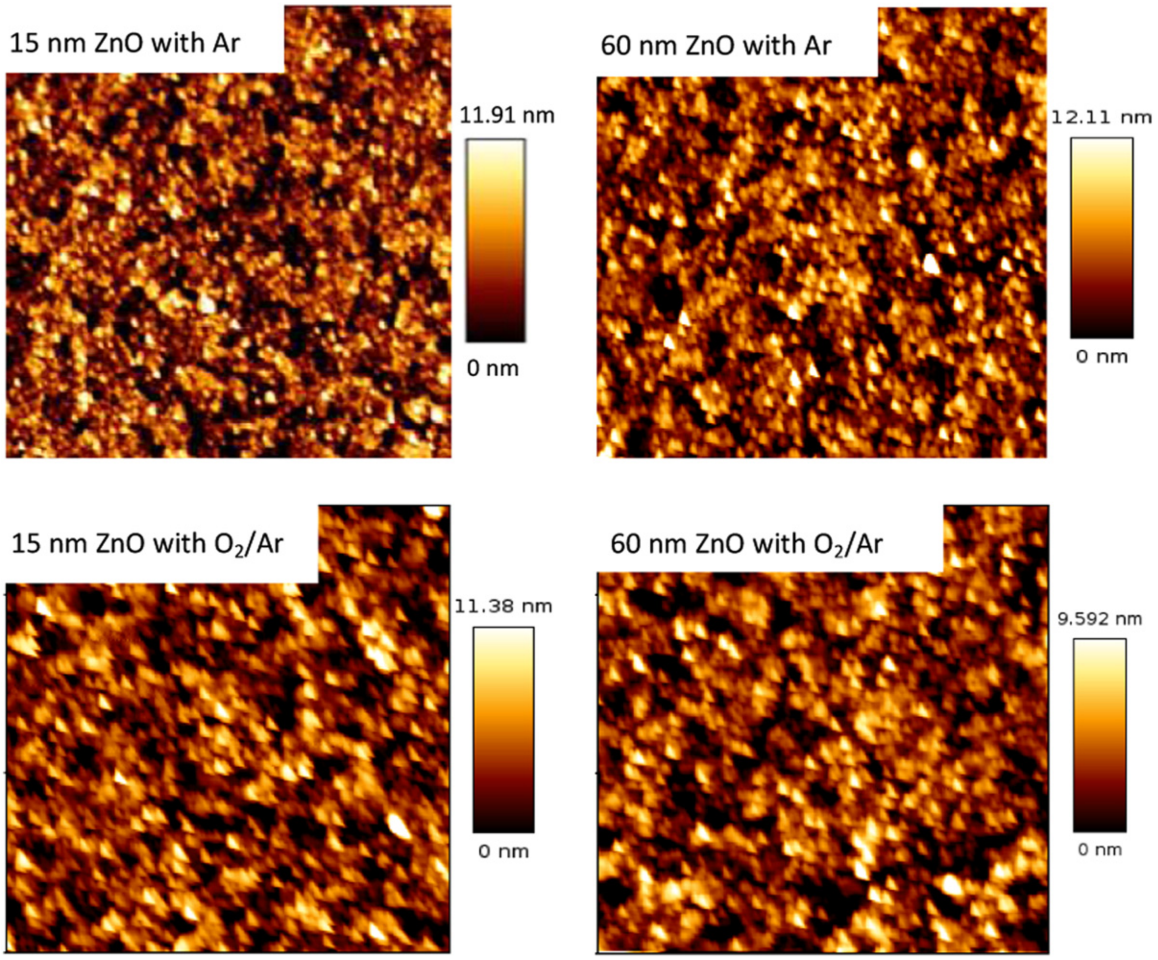

Figure 5. AFM surface morphologies of 15 nm and 60 nm ZnO films sputtered with Ar and O_2/Ar (1:7) gas, respectively.

That means that the forming progress of first-step sputtered ZnO layer can be adjusted while sputtering the second-step ZnO layer due to changing O_2/Ar ratio gas [25]. Naturally some defects, such as pinholes, in the first-step ZnO layer can be inhibited or displaced when depositing the second ZnO layer. Therefore, the numbers of pinholes penetrated into the whole ZnO layer are expected to greatly reduce, which can decrease the reverse saturation current and improve shunt resistance of PSCs.

Electron transport ability of bulk ZnO layer is also another important factor for influencing the performance of PSCs [14, 32]. The high bulk resistance can lead to electron strictly unbalancing distribution in the bulk ZnO layer, which can limit carrier injection from photoactive layer and increase electron accumulation at the ZnO/P3HT:PCBM interface. However, this relatively low electron accumulation effect in PSCs with totally thick, less than 30 nm ZnO layer, cannot be observed due to limitation of impedance spectroscopy, as shown in figures 3(a)–(c). The bulk resistance effect of ZnO layer can be enlarged through increasing ZnO layer thickness. Compared to impedance spectra of PSCs with 30 nm and 60 nm ZnO layers, the negative capacitance of PSC with O_2/Ar single-step sputtered 60 nm ZnO layer in figure 3(d) is at least partly attributed to high bulk resistance of 60 nm thick ZnO layer, which

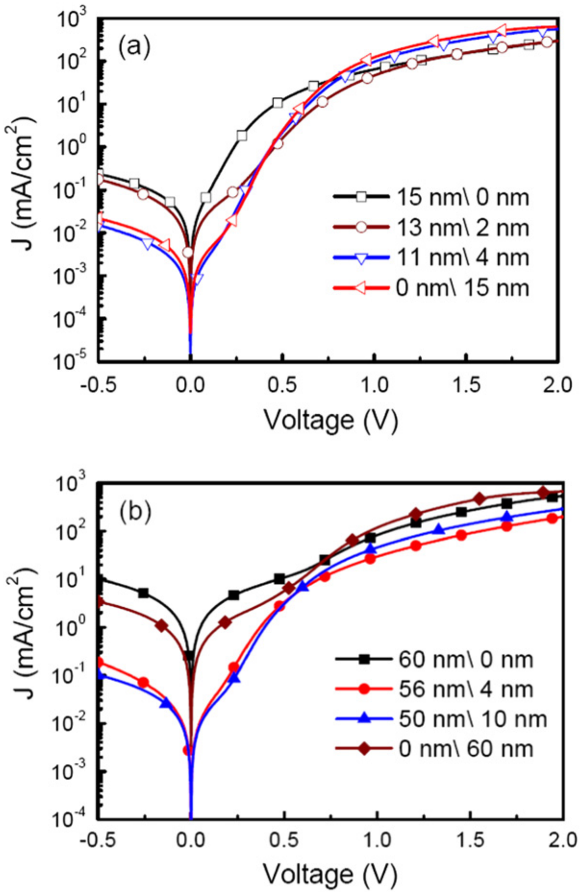

Figure 6. Dark *J*–*V* curves of PSCs with X (nm)\Y (nm) ZnO layer.

results in electron accumulation at the ZnO/P3HT:PCBM interface [26]. The weaker negative capacitance effect of PSCs with 50 nm/10 nm ZnO layer suggested that electron accumulation at the ZnO/P3HT:PCBM interface was attenuated due to low bulk resistance of the first-step 50 nm ZnO layer.

4. Conclusion

The efficient inverted PSCs with ZnO as cathode interfacial layer have been demonstrated by two-step magnetron sputtered ZnO layer. The PCE of PSCs with 11 nm/4 nm ZnO layer reaches 4.08%, which is obviously higher than that of PSCs with 15 nm ZnO layer sputtered with O_2/Ar ratio (1:7) gas. The first-step ZnO layer sputtered with Ar gas shows lower bulk resistance and improves its electron transport ability. The right thickness second-step ZnO layer sputtered with O_2/Ar (1:7) gas can obtain superior surface properties and improve CB levels due to oxygen gas participation. The defects penetrating into the whole ZnO cathode interfacial layer can be inhibited or displaced by two-step sputtered ZnO layer method. The two-step sputtered ZnO layer strategy has an integrated advantage of decreasing energy difference between ZnO and PCBM, inhibiting defects penetrated into the whole ZnO layer, improving surface properties and enhancing carrier transport ability of ZnO cathode interfacial layer compared to ZnO layer sputtered with Ar gas or O_2/Ar gas.

Acknowledgment

This work was supported by National Natural Science Foundation of China (grant Nos. 61275038, 11274119), Doctoral Fund of Ministry of Education of China (grant No.20110076120017) and SRF for ROCS, SEM.

References

[1] Espinosa N, Hösel M, Angmo D and Krebs F C 2012 Solar cells with one-day energy payback for the factories of the future *Energy Environ. Sci.* **5** 5117–32

[2] He M, Han W, Ge J, Yang Y, Qiu F and Lin Z 2011 All-conjugated poly (3-alkylthiophene) diblock copolymer-based bulk heterojunction solar cells with controlled molecular organization and nanoscale morphology *Energy Environ. Sci.* **4** 2894–902

[3] He M, Han W, Ge J, Yu W, Yang Y, Qiu F and Lin Z 2011 Annealing effects on the photovoltaic performance of all-conjugated poly (3-alkylthiophene) diblock copolymer-based bulk heterojunction solar cells *Nanoscale* **3** 3159–63

[4] He M, Qiu F and Lin Z 2013 Toward high-performance organic–inorganic hybrid solar cells: bringing conjugated polymers and inorganic nanocrystals in close contact *J. Phys. Chem. Lett.* **4** 1788–96

[5] Zhou N, Guo X, Ortiz R P, Li S, Zhang S, Chang R P, Facchetti A and Marks T J 2012 Bithiophene imide and benzodithiophene copolymers for efficient inverted polymer solar cells *Adv. Mater.* **24** 2242–8

[6] You J, Dou L, Yoshimura K, Kato T, Ohya K, Moriarty T, Emery K, Chen C-C, Gao J and Li G 2013 A polymer tandem solar cell with 10.6% power conversion efficiency *Nat. Commun.* **4** 1446

[7] He Z, Zhong C, Su S, Xu M, Wu H and Cao Y 2012 Enhanced power-conversion efficiency in polymer solar cells using an inverted device structure *Nat. Photonics* **6** 593–7

[8] He M, Wang M, Lin C and Lin Z 2014 Optimization of molecular organization and nanoscale morphology for high performance low bandgap polymer solar cells *Nanoscale* **6** 3984–94

[9] Guo X, Zhou N, Lou S J, Smith J, Tice D B, Hennek J W, Ortiz R P, Navarrete J T L, Li S and Strzalka J 2013 Polymer solar cells with enhanced fill factors *Nat. Photonics* **7** 825–33

[10] Irwin M D, Buchholz D B, Hains A W, Chang R P H and Marks T J 2008 P-type semiconducting nickel oxide as an efficiency-enhancing anode interfacial layer in polymer bulk-heterojunction solar cells *Proc. Nat. Acad. Sci.* **105** 2783–7

[11] Kyaw A, Sun X, Jiang C, Lo G, Zhao D and Kwong D 2008 An inverted organic solar cell employing a sol-gel derived ZnO electron selective layer and thermal evaporated MoO3 hole selective layer *Appl. Phys. Lett.* **93** 221107

[12] Chen X, Yang J, Haley L Y X C, Lu J, Zhu F and Loh K P 2010 Towards high efficiency solution processable inverted bulk heterojunction polymer solar cells using modified indium tin oxide cathode *Org. Electron.* **11** 1942–6

[13] He Z, Zhong C, Huang X, Wong W Y, Wu H, Chen L, Su S and Cao Y 2011 Simultaneous enhancement of open-circuit voltage, short-circuit current density, and fill factor in polymer solar cells *Adv. Mater.* **23** 4636–43

[14] You J, Chen C C, Dou L, Murase S, Duan H S, Hawks S A, Xu T, Son H J, Yu L and Li G 2012 Metal oxide nanoparticles as an electron-transport layer in high-performance and stable inverted polymer solar cells *Adv. Mater.* **24** 5267–72

[15] Hau S K, Yip H-L, Baek N S, Zou J, O'Malley K and Jen A K-Y 2008 Air-stable inverted flexible polymer solar cells using zinc oxide nanoparticles as an electron selective layer *Appl. Phys. Lett.* **92** 253301

[16] Barankin M, Gonzalez I E, Ladwig A and Hicks R 2007 Plasma-enhanced chemical vapor deposition of zinc oxide at atmospheric pressure and low temperature *Sol. Energy Mater. Sol. Cells* **91** 924–30

[17] Cheun H, Fuentes-Hernandez C, Zhou Y, Potscavage W J Jr, Kim S-J, Shim J, Dindar A and Kippelen B 2010 Electrical and optical properties of ZnO processed by atomic layer deposition in inverted polymer solar cells† *J. Phys. Chem.* C **114** 20713–8

[18] Jouane Y, Colis S, Schmerber G, Dinia A, Lévêque P, Heiser T and Chapuis Y-A 2013 Influence of flexible substrates on inverted organic solar cells using sputtered ZnO as cathode interfacial layer *Org. Electron.* **14** 1861–8

[19] Zhu F, Chen X, Lu Z, Yang J, Huang S and Sun Z 2014 Efficiency enhancement of inverted polymer solar cells using ionic liquid-functionalized carbon nanoparticles-modified ZnO as electron selective layer *Nano-Micro Lett.* **6** 24–9

[20] Zhu F, Chen X, Zhou L, Zhou J, Yang J, Huang S and Sun Z 2014 Dependence of the performance of inverted polymer solar cells on thickness of an electron selective ZnO layer deposited by magnetron sputtering *Thin Solid Films* **551** 131–5

[21] Park Y S, Choi K H and Kim H K 2009 Room temperature flexible and transparent ITO/Ag/ITO electrode grown on flexile PES substrate by continuous roll-to-roll sputtering for flexible organic photovoltaics *J. Phys. D: Appl. Phys.* **42** 235109

[22] Guillén C and Herrero J 2011 TCO/metal/TCO structures for energy and flexible electronics *Thin Solid Films* **520** 1–17

[23] Zhou L, Chen X, Zhu F, Sun X X and Sun Z 2012 Improving temperature-stable AZO–Ag–AZO multilayer transparent electrodes using thin Al layer modification *J. Phys. D: Appl. Phys.* **45** 505103

[24] Jouane Y, Colis S, Schmerber G, Kern P, Dinia A, Heiser T and Chapuis Y-A 2011 Room temperature ZnO growth by rf magnetron sputtering on top of photoactive P3HT: PCBM for organic solar cells *J. Mater. Chem.* **21** 1953–8

[25] Jeong W-J and Park G-C 2001 Electrical and optical properties of ZnO thin film as a function of deposition parameters *Sol. Energy Mater. Sol. Cells* **65** 37–45

[26] Garcia-Belmonte G, Munar A, Barea E M, Bisquert J, Ugarte I and Pacios R 2008 Charge carrier mobility and lifetime of organic bulk heterojunctions analyzed by impedance spectroscopy *Org. Electron.* **9** 847–51

[27] Leever B J, Bailey C A, Marks T J, Hersam M C and Durstock M F 2012 *In situ* characterization of lifetime and morphology in operating bulk heterojunction organic photovoltaic devices by impedance spectroscopy *Adv. Energy Mater.* **2** 120–8

[28] Gwinner M C, Vaynzof Y, Banger K K, Ho P K, Friend R H and Sirringhaus H 2010 Solution-processed zinc oxide as high-performance air-stable electron injector in organic Ambipolar light-emitting field-effect transistors *Adv. Funct. Mater.* **20** 3457–65

[29] Schleife A, Fuchs F, Rödl C, Furthmüller J and Bechstedt F 2009 Branch-point energies and band discontinuities of III-nitrides and III-/II-oxides from quasiparticle band-structure calculations *Appl. Phys. Lett.* **94** 012104

[30] Allen M, Swartz C, Myers T, Veal T D, McConville C F and Durbin S 2010 Bulk transport measurements in ZnO: the effect of surface electron layers *Phys. Rev.* B **81** 075211

[31] Green R, Morfa A, Ferguson A, Kopidakis N, Rumbles G and Shaheen S 2008 Performance of bulk heterojunction photovoltaic devices prepared by airbrush spray deposition *Appl. Phys. Lett.* **92** 033301

[32] Liang Z, Zhang Q, Wiranwetchayan O, Xi J, Yang Z, Park K, Li C and Cao G 2012 Effects of the morphology of a ZnO buffer layer on the photovoltaic performance of inverted polymer solar cells *Adv. Funct. Mater.* **22** 2194–201